Clim Dyn (2018) 51:3985–3998
DOI 10.1007/s00382-017-3691-0

Intraseasonal responses of the East Asia summer rainfall to anthropogenic aerosol climate forcing

Guoxing Chen[1] · Jing Yang[2] · Qing Bao[3] · Wei-Chyung Wang[1]

Received: 31 October 2016 / Accepted: 13 April 2017 / Published online: 22 April 2017

Abstract The WRF Model is used to investigate intraseasonal responses of the summer rainfall to aerosol direct and cloud-adjustment effects over East Asia, where the anthropogenic aerosol loading has been increasing in the past few decades. The responses are evaluated by comparing two cases for each year during 2002–2008: a control case imposing the observed aerosol optical depth of the corresponding year and a sensitivity case having anthropogenic components of the control case reduced by 75%. Analyses of multiple-year simulations reveal that aerosol-induced changes of rainfall and circulation exhibit strong intraseasonal variability, and that the spatial pattern of changes in the monthly rainfall is related to the intensification and westward extension of the western North-Pacific subtropical high (WNPSH) by increased aerosols. This perturbation of the WNPSH induces surface air divergence over the southeast China and convergence over regions to the north and west of the WNPSH, causing, respectively, decreased and increased rainfall. As the WNPSH migration path varies year by year, however, the variability of rainfall changes over subregions of the eastern China (e.g., North China) is large within the decade. Meanwhile, the pattern of summer-gross rainfall changes also shows large interannual variation, but the general pattern of wetter in the west and dryer in the east persists. Results also suggest that the aerosol increase tends to reduce the number of Tibet Plateau vortices, which indirectly influence summer rainfall over the eastern China.

Keywords Intraseasonal · Aerosol climate forcing · East Asia summer monsoon · Western North-Pacific subtropical high

1 Introduction

Aerosol effects in the climate system are highly buffered by strong multiscale coupling between aerosol, cloud, radiation, meteorology and human activities (Stevens and Feingold 2009). Consequently, climate responses to aerosol perturbations might exhibit different characteristics for various temporal scales. For instance, for short time (cloud/synoptic) scales, increasing aerosol concentration tends to suppress the warm-phase precipitation and enhance the mixed-phase precipitation, and the net precipitation can be either increased or decreased (e.g., Rosenfeld et al. 2008; Li et al. 2011a); nevertheless for long time (interannual/decadal) scales, higher aerosol loading tends to weaken the monsoon and reduce the surface precipitation by reducing the land surface temperature and thus the temperature gradient between land and ocean (e.g., Ramanathan et al.

This paper is a contribution to the special issue on East Asian Climate under Global Warming: Understanding and Projection, consisting of papers from the East Asian Climate (EAC) community and the 13th EAC International Workshop in Beijing, China on 24–25 March 2016, and coordinated by Jianping Li, Huang-Hsiung Hsu, Wei-Chyung Wang, Kyung-Ja Ha, Tim Li, and Akio Kitoh.

✉ Wei-Chyung Wang
wcwang@albany.edu

[1] Atmospheric Sciences Research Center, University at Albany, State University of New York, Albany 12203, NY, USA

[2] State Key Laboratory of Earth Surface Processes and Resource Ecology, Faculty of Geographical Science, Beijing Normal University, Beijing, China

[3] State Key Laboratory of Numerical Modeling for Atmospheric Sciences and Geophysical Fluid Dynamics, Institute of Atmospheric Sciences, Chinese Academy of Sciences, Beijing, China

2001). Previous studies usually examine climate responses to aerosol perturbations at these two kinds of extreme scales, while still few take care of the responses at scales between them—the intraseasonal and interseasonal scales. Because the atmospheric intraseasonal variations are highly linked to various disastrous weather events during the summer (e.g., Hong et al. 2010; Liu et al. 2014), this study aims to investigate intraseasonal characteristics of aerosol effects on the summer rainfall over East Asia, where the summer monsoon dominates the annual precipitation.

Intraseasonal variations widely exist in the East Asia climate system, and play an important role in the development of many weather events. For example, the quasi-biweekly oscillation has been identified in the summer precipitation over the Tibet Plateau (TP) (Wang and Duan 2015; Yang et al. 2016), North China (Yang et al. 2014) and the Lower Reach of Yangtze Basin (Yang et al. 2010). Liu et al. (2014) showed that the extreme heavy rainfall over the southern Yangtze and Huai River Basin in the summer of 2008 was induced by the superposition of quasi-biweekly and synoptic-scale disturbances. Similarly, Hong et al. (2010) showed that the extreme rainfall event associated with Typhoon Morakot (2009) in Southern Taiwan resulted from the superposed cyclonic phases of the 10–30-day and 40–50-day intraseasonal oscillations. Recently, Zhang et al. (2014) claimed that the quasi-biweekly oscillation over the TP highly modulates the activity of TP vortices (TPVs), many of which propagate eastward and develop into precipitating systems over the eastern China in summer (Tao and Ding 1981).

The aerosol loading over Asia has been rapidly increasing in the past 30 years due to industrialization and urbanization (Li et al. 2011b; Wang et al. 2015). A wide range of theoretical, observational and modeling studies have been carried out on aerosol climate effects on Asian monsoons and the associated precipitation as listed in the recent study by Li et al. (2016b). Here we only give a brief review on major findings. On the continental scale, increased aerosols reduce the surface insolation by aerosol direct and indirect effects, cooling the continent and weakening the monsoon (e.g., Guo et al. 2013; Li et al. 2016a). Locally, aerosols alter thermodynamic profiles via radiative effects, which modulates cloud formation and local circulation (e.g., Wang et al. 2013b; Yang et al. 2013a, b), and change cloud albedo and precipitation susceptibility by acting as cloud and ice nuclei (e.g., Cheng et al. 2010; Fan et al. 2012). Particularly, a few studies have pointed out the intraseasonal characteristics of aerosol effects on the Indian summer monsoon precipitation. For example, Lau and Kim (2006) and Lau et al. (2006) showed that increased absorbing aerosols may induce an advance of rainy periods and intensify the summer monsoon via the 'Elevated Heat Pump' mechanism; and Manoj et al. (2011) claimed that absorbing aerosols tend to facilitate transition of the monsoon from break to active spells. In contrast, the intraseasonal characteristics of aerosol effects on the East Asia summer rainfall have not been addressed yet.

In this study, we simulate the summer rainfall over East Asia using the WRF Model, in which both direct and indirect effects of aerosols are calculated online, and examine the characteristics of the monthly-rainfall responses to the anthropogenic aerosol perturbation. Previous studies have shown that the rainbelt over East Asia is generally characterized by the northward marching month by month with the successive onset of the summer monsoon from South China to North China (e.g., Qian and Lee 2000). In May, the rainbelt starts to form over South China; in June, it shifts to the Yangtze/Huai River Valley (YHRV) when the Meiyu starts; then in July, it moves further northward, and finally retreats from Northeastern China at the end of August (Dao and Chen 1957). Besides, interannual variability also exists in the rainbelt marching. When the northwest subtropical ridge is intensified and westward extended, the Meiyu lasts a longer time over the YHRV and produces more precipitation there (Chang et al. 2000).

The rest of this paper is arranged as follows: detailed descriptions of the model and experiment setup are given in Sect. 2; Sect. 3 shows the characteristics of the simulated monthly precipitation and cloud; Sect. 4 presents the characteristics of aerosol effects on the monthly surface rainfall and its interannual variability; and the conclusion and discussion are given in Sect. 5.

2 Model and experiment setup

2.1 Model configuration

In this study, aerosol direct and indirect effects are online calculated in the WRF Model (version 3.6.1). Multi-component aerosol fields are prescribed to account for aerosol radiative effects; meanwhile, soluble aerosol components are converted into the equivalent ammonia-sulfate mass based on their hygroscopicity and serve as cloud nuclei (CN) in a two-moment cloud microphysical scheme (Cheng et al. 2007, 2010; Chen et al. 2015; Chen and Wang 2016), which predicts number and mass mixing ratios of five hydrometeor classes (cloud droplet, rain droplet, cloud ice, snow and graupel). Whenever the radiation transfer subroutines are called (every 30 min), the model calculates aerosol radiative properties with the instant relative humidity using subroutines imported from the WRF-Chem Model, and effective radii of cloud droplet, cloud ice and snow with the predicted number and mass mixing ratios of relevant hydrometeors, and then passes them to the RRTMG shortwave and longwave radiation schemes (Iacono et al.

2008) together with hydrometeor mass mixing ratios. The effective radius of cloud droplet is calculated with the formula in Chen and Liu (2004), while effective radii of cloud ice and snow are calculated using codes from the Thompson scheme (Thompson et al. 2016). In addition, because this microphysical scheme tracks CN mass in hydrometeors, CN at each cubic grid can be depleted by cloud and precipitation processes, and its concentration recovers to the prescribed level only when the gird is cloud free. In this way, CN removal due to cloud and precipitation processes is accounted for to some degree, avoiding nucleating too many droplets. Ice nucleation is calculated with empirical equations (see details in Cheng et al. 2010) and is not affected by the prescribed aerosol fields, thus aerosols' role as ice nuclei is not concerned in this study.

Other physical processes are configured using the default model setup: the Kain-Fritsch scheme (Kain 2004) for cumulus convection, the Noah scheme (Chen and Dudhia 2001) for land surface, the Monin–Obukhov scheme (Monin and Obukhov 1954) for surface layer and the YSU scheme (Hong et al. 2006) for planetary boundary layer, respectively. Note that the cumulus radiative feedback is deactivated, so neither cloud fraction nor condensate masses from the cumulus parameterization intervene in the radiation calculation. This contributes the underestimation of liquid water path (LWP) shown below.

Figure 1 presents the simulation domain. Besides East Asia, the domain includes a part of South Asia (the northern India). It is expected that the Indian aerosol loading might affect the TPV activities and subsequently modulate precipitating systems over East Asia. There are 201×140 grids horizontally with a resolution of 30 km and 50 levels vertically. Note that with the current horizontal resolution, cumulus parameterization handles most precipitation while microphysical parameterization can only resolve large-scale stratus clouds, which produce less precipitation but dominate cloud radiative forcing. Therefore, aerosol effects of precipitation suppression (Albrecht 1989) and convection invigoration (Rosenfeld et al. 2008) are minimal in this study, and changes of cloud and precipitation are mainly attributed to adjustments to stability and circulation changes caused by shortwave cooling associated with aerosol direct (radiative) and first-indirect (Twomey 1974) effects and longwave warming associated with aerosol-perturbed ice content in stratus clouds (Fan et al. 2016; Wang et al. 2014).

The model is driven with meteorological forcings from the ERA-Interim Reanalysis (Dee et al. 2011; http://rad.ucar.edu/datasets/ds627.0), and the daily SST from the NCEP RTG_SST analysis data (Thiébaux et al. 2003).

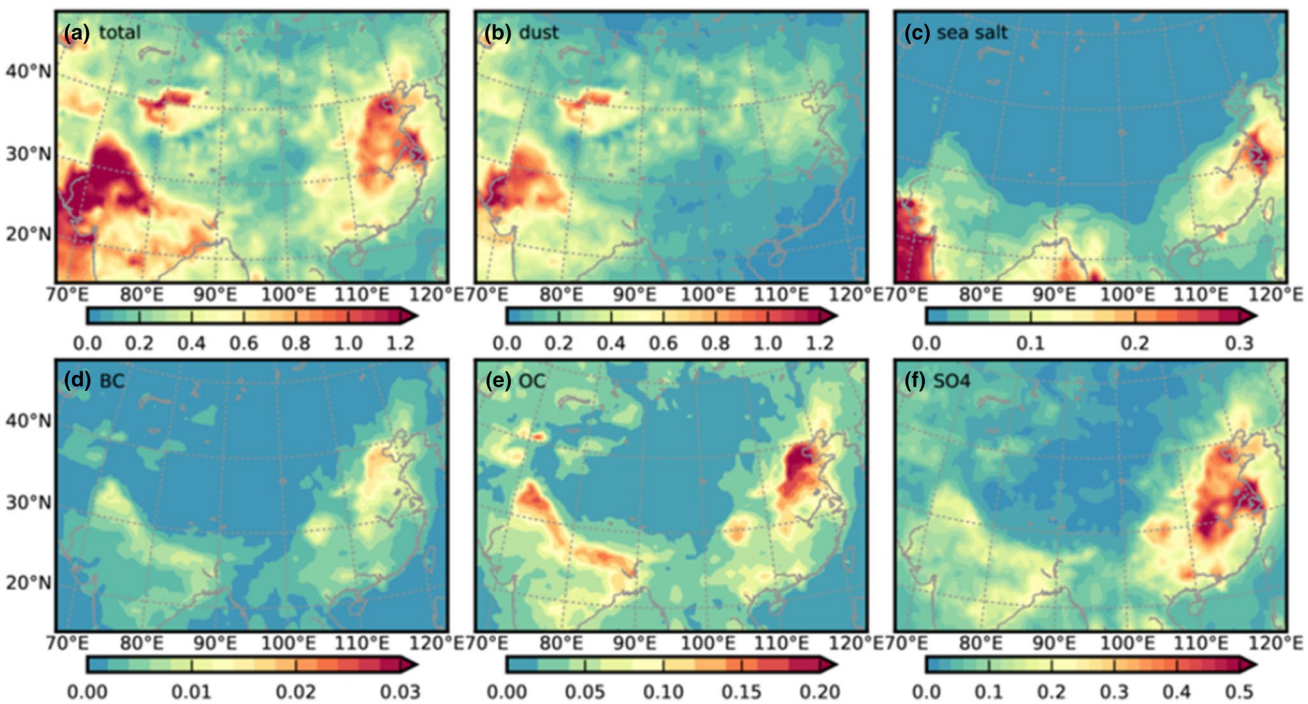

Fig. 1 Aerosol optical depth (AOD) in the control simulation of 2008: **a** total AOD; **b–f** AOD of dust, sea salt, black carbon (BC), organic carbon (OC) and sulfate (SO4) aerosols, respectively

2.2 Experiment setup

The summer climate over East Asia is simulated for 7 years (2002–2008), and its responses to aerosols are examined for each year individually. This is intentional because the East Asia summer monsoon (EASM) exhibits strong interannual variability in both intensity and duration. As shown by Li et al. (2016a; cf. Fig. 1), the EASM is relatively strong in 2002, 2004 and 2006 but weak in the rest 4 years. Climate responses might show different characteristics in different years even for the same aerosol forcing, and conventional composite analyses between years could mask these characteristics to some degree. For all years, the simulation runs from 28 May to 31 August with data stored every 3 h, and results in the first 4 days are discarded as the model spin-up. For 2008, two extra simulations are conducted with a different initial time (2008-05-26 12:00:00 UTC) and a different computer to improve the robustness. The results show sensitivity to these conditions (shown in Sect. 4), but retain similar intraseasonal characteristics. It gives us the confidence to examine the interannual variability of these characteristics using data from the single-ensemble simulations for other years.

For each year, intraseasonal responses are evaluated by comparing two cases: a control case and a sensitivity case, which are representative of the current (polluted) aerosol loading and the aerosol loading in 1970s before the rapid industry growth over Asia, respectively. In the control case, aerosol fields in the WRF model are composited using the historical aerosol data from the CAM-Chem Model (Lamarque et al. 2012) and the observed aerosol optical depth (AOD) by the Aqua MODIS instrument (v051, Level 3, monthly). The CAM-Chem aerosol data have monthly mixing ratios of 14 components for 5 aerosol species including sulfate, black carbon (BC), organic carbon (OC), sea salt and dust. Because the AOD calculated with this dataset shows large deviations from the MODIS AOD in both the spatial distribution and magnitude (figure not shown), we multiply aerosol concentrations in each column with a factor to make the resulted AOD match the MODIS AOD. In other words, the MODIS data provide information of aerosol horizontal distribution, while the CAM-Chem data provide information of aerosol vertical distribution and chemistry compositions. The monthly aerosol fields vary little during 3 months in summer (June–August), so we simply employ the summer-mean aerosol loading in the model and hold it constant throughout the simulation. Aerosol temporal variations are mainly significant at the synoptic scale (~days) and cannot be resolved by the monthly data in this study. Their climate effects will be investigated by using aerosol data with finer time resolutions in our future research.

Figure 1 presents the AOD distribution in the control case of 2008, and the similar spatial patterns persist in the control case of other years (figure not shown). Three peak regions are identified: the India subcontinent, the Tarim Basin and the eastern China (Fig. 1a). Large AOD values over the Tarim Basin and the northwest India are dominated by dust particles (Fig. 1b), while large AOD values over the northern India (along the south slope of the Himalayas) and the eastern China are dominated by BC, OC and sulfate (Fig. 1d–f). The latter regions generally correspond to concentrated areas of cities and industries (e.g., the Jing-Jin-Ji region and the YHRV), in line with the dominance of anthropogenic emissions in BC, OC and sulfate aerosols. The AOD by sea salt only shows large values over the ocean and coastal regions, and is negligible over the inland.

In the sensitivity case, the multi-component aerosol fields are identical to those in the control case, except that the concentrations of anthropogenic aerosols (sulfate, OC and BC) are reduced to their 1/4. This simple estimation for the aerosol loading in 1970s is not fully arbitrary. As shown in Fig. 2a, the SO_2 emission rate in 2000s by China mainland and India is approximately 4 times that in 1970s.

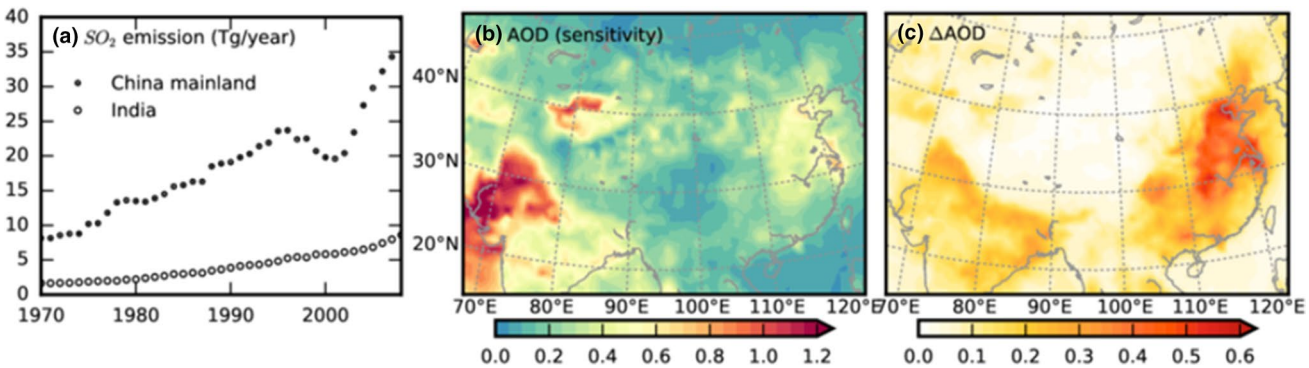

Fig. 2 Configurations of aerosol loading in the sensitivity case of 2008: **a** historical anthropogenic SO_2 emission rates of China mainland and India in 1970–2008; **b** total AOD in the sensitivity case; **c** difference in total AOD between control and sensitivity cases (control minus sensitivity). Source of SO_2 emission rate: EC-JRC/PBL. EDGAR version 4.2. http://edgar.jrc.ec.europa.eu/, 2011

Since emissions of sulfate, OC and BC are associated with the same set of human activities, it is assumed in this configuration that the loadings of aerosols are proportional to their emission rates, and the SO_2 emission rate indicates the emission level of all anthropogenic aerosols. As a result, the AOD difference between control and sensitivity cases is significant over the northern India and the eastern China but minor over other regions (Fig. 2b, c). The focus of this study is how this pattern of aerosol perturbations affects the surface precipitation.

3 Characteristics of the simulated monthly precipitation and cloud

This section presents a general perspective of the ensemble-mean results from the control simulations of 2008 to demonstrate the model's performance in simulating the monsoon intraseasonal migration and the associated changes in precipitation and cloud.

Figure 3 shows the monthly-mean rain rate from WRF simulations compared with the rain rate estimated by the ERA-Interim 12-hour forecast and the Global Precipitation Climatology Project (GPCP, Version 1.2; Huffman et al. 2001). For all 3 months, the rain rate from WRF simulation is much higher than that in GPCP, but is very close to that in ERA-Interim forecast. It indicates that parameterizations in the WRF Model well capture responses of circulation and precipitation to meteorological forcings from the ERA-Interim reanalysis, but the ERA-Interim itself has some uncertainties over East Asia relative to observations. The overestimated precipitation is also shown in Li et al. (2016a; cf. Fig. 2), where the ERA-Interim data were used to drive a different regional climate model.

From June to August, the simulated rainbelt migration by WRF is quite similar to that shown in ERA-Interim

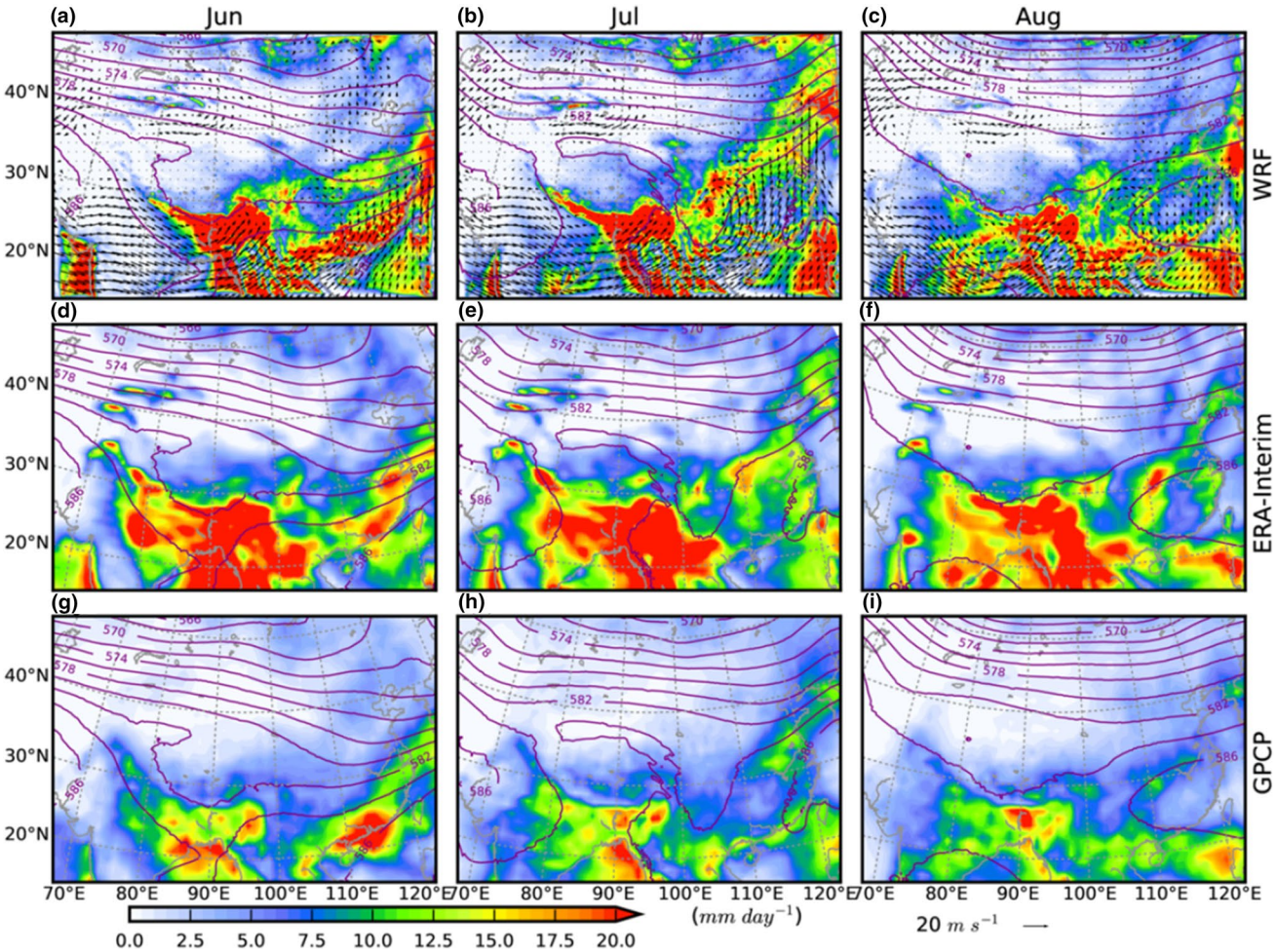

Fig. 3 Monthly-mean rain rate in the 2008 summer from **a** the WRF simulation (the control case), **b** the ERA-Interim forecast and **c** the GPCP dataset. *Purple lines* in this figure, Figs. 4, 5, 6, 7, 8 and 10 indicate simulated 500 hPa geopotential height fields in the control case (unit 10 gpm)

and GPCP datasets. In June, when the western North-Pacific subtropical high (WNPSH) is just touching the southeast coast of China (5860 contour in Fig. 1a), a rainbelt is formed over the southeast China. The strong southwest air flow (wind fields at 850 hPa) brings large amounts of water vapor there from the South China Sea. Meanwhile, another rainbelt is starting to form over the YHRV. In July, when the WNPSH is extended westward and northward and occupies the southeast coast, the rainfall over the southeast China is much reduced while the YHRV rainbelt is enhanced and shifted northwestward to some degree. The southwest flow at 850 hPa also gets deep into North China. In August, when the WNPSH extends further westward to the inland China and begins to retreat southward, precipitation is suppressed over the whole South China while the rainbelt over North China is still visible but much weaker. As the southwest flow is greatly weakened, excessive water vapor is confined over the tropical land and ocean, where heavy precipitation is produced.

Overall, it is shown that the rainbelt marching over the eastern China is driven by the WNPSH intraseasonal migration. For all months, the heavy rainfall tends to occur over regions to the west and north of the WNPSH, where the water vapor is convergent; and less rainfall is produced over regions dominated by the WNPSH and divergent flows.

As aerosol indirect radiative forcing is mainly relevant to liquid clouds, here we evaluate the simulated cloud fraction below 440 hPa (where most liquid water resides) and LWP against the observed LWP by Aqua MODIS. Shown in Fig. 4, the model underestimates LWP over many regions by as much as 100 g m^{-2}. This is not unexpected. As noted in Sect. 2.1, the simulated clouds are composed of only large-scale stratus clouds due to the coarse horizontal resolution, and convective clouds, which are usually smaller than the grid size but carry large amounts of cloud water, are excluded. Certainly this tends to lower the simulated shortwave radiative forcing. However, the liquid clouds present the similar intraseasonal characteristics as the surface rainfall for both simulations and observations: cloud fraction and LWP are large over regions to the west and north of the WNPSH and small over the WNPSH occupied region. It is clear that clouds are concentrated to the south of 35°N in June, and move northward in July and August when cloud cover and thickness are much reduced over the southeast China due to the WNPSH occupation. As a result, the indirect radiative forcing of aerosols should be strong to the west and north of the WNPSH. This is shown below to have contributions to the rainfall responses to aerosol perturbations.

4 Aerosol effects on the summer rainfall

In this section, we examine the intraseasonal responses of surface rainfall and circulation to anthropogenic aerosol perturbations by comparing results from the control and sensitivity simulations for each individual year. Firstly, the characteristics of monthly-mean responses are demonstrated using the ensemble-mean results from simulations of 2008; then results from simulations of other years are used to verify these characteristics to account for interannual variations of the EASM.

4.1 Intraseasonal characteristics of changes in rainfall and circulation

Figure 5 presents responses of the monthly-mean rainfall at the surface during 2008, in which the 500 hPa geopotential height fields from the control case are superposed (the purple contours) to facilitate analyses. First, it is clear that the total rainfall changes do not have a constant spatial pattern (e.g., flooding in south and drought in north) in the 3 months in spite of the constant aerosol perturbation (Fig. 5a–c). Instead, the spatial pattern exhibits strong variations associated with the intraseasonal migration of the WNPSH: the boundaries between regions with increased and decreased precipitation move northward and westward with the WNPSH. For all months, the WNPSH occupied regions (i.e. southeast coast in June and South China in July and August) are characterized by reduced precipitation, while regions to the west and north of the WNPSH are characterized with enhanced precipitation. Second, changes of convective rainfall (Fig. 5d–f) dominate the total rainfall changes, which is in line with that convective rainfall dominates total rainfall due to the coarse horizontal resolution. Third, changes of convective and stratus (microphysical, Fig. 5g–i) rainfalls generally have the same spatial distributions as the total rainfall changes. This is because aerosol effects of precipitation suppression and convection invigoration are not significant in the current model setup, and thus rainfall changes are dominated by the meteorology perturbation due to circulation changes. Particularly for the stratus rainfall, it can be inferred that the effect of circulation changes overwhelms the aerosol effect of precipitation suppression.

Changes of liquid cloud fraction and LWP show similar spatial patterns to those of precipitation (Fig. 6). When anthropogenic aerosols are increased, cloud cover and thickness are increased to the west and north of the WNPSH but decreased over the WNPSH occupied regions. Therein, changes of mid-level clouds (between 680 and 440 hPa) dominate; low-level clouds (below 680 hPa) are generally increased over the whole eastern China; and changes of high-level clouds (above 440 hPa) are similar

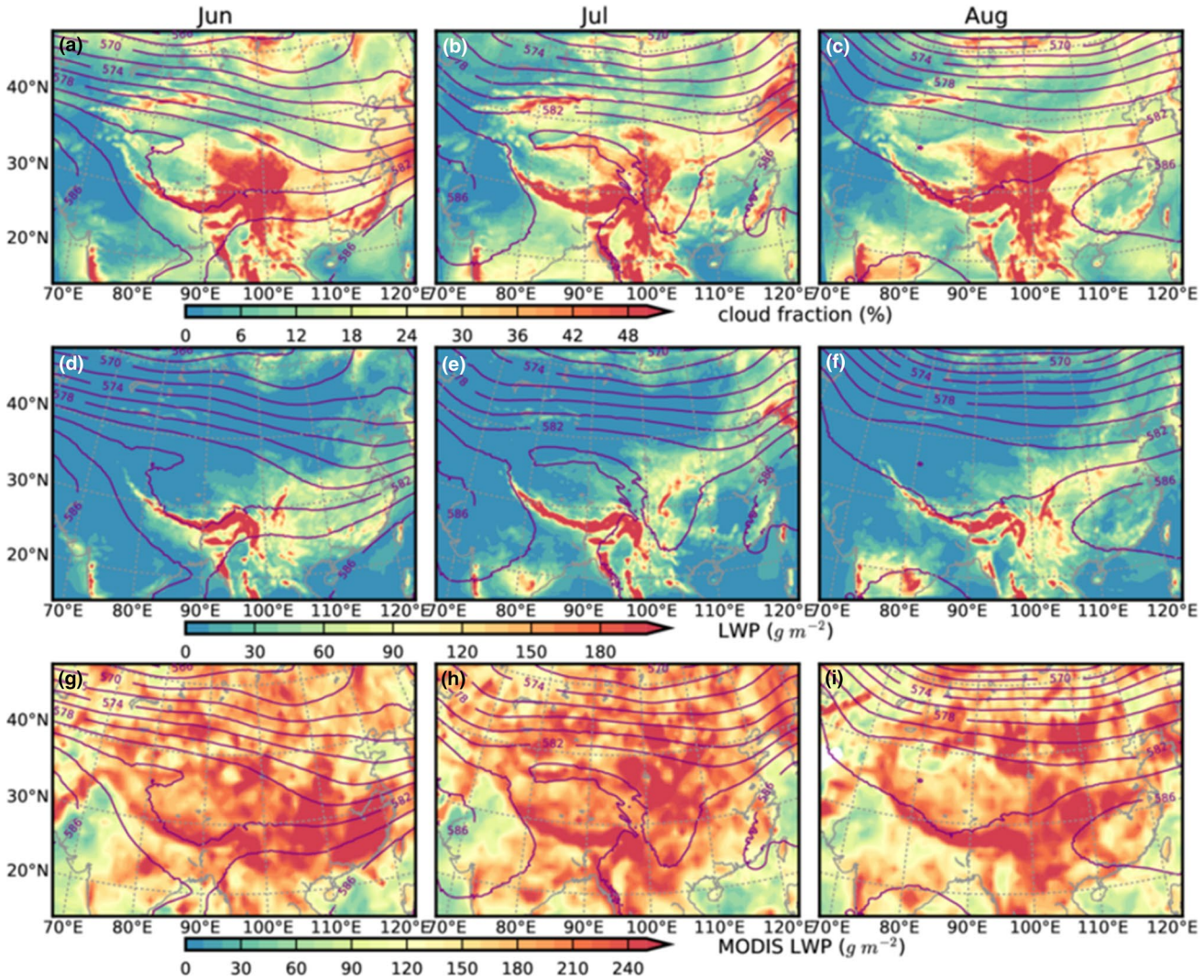

Fig. 4 Monthly cloud fraction (below 440 hPa) and liquid water path (LWP) from control simulations of 2008. The columnar cloud fraction **a–c** is calculated assuming maximum/random overlapping using only 3D cloud fraction below 440 hPa, for low- and mid-level clouds contain most liquid water and dominate the shortwave cloud radiative forcing. MODIS LWP data are from the Aqua satellite (MYD08_M3_6, 1°×1°; from https://giovanni.sci.gsfc.nasa.gov/). Note that the lower two rows use *different colorbar* ranges to highlight the similarity of cloud spatial distributions

to those of mid-level clouds (figure not shown). Given that the simulated clouds are composed of only stratus clouds while the simulated precipitation is dominated by convective clouds, this further confirms that the responses are dominated by adjustment to circulation changes.

Figure 7 shows aerosol forcings on the surface energy balance via direct (aerosol–radiation interaction) and indirect (aerosol–cloud–radiation interactions) paths. The pattern of direct radiative forcing (ΔDRF, Fig. 7a–c) is in line with that of the AOD difference (i.e. Fig. 2c), and shows little variation from June to August. For most regions (especially the northern India and the eastern China), the aerosol perturbation reduces radiation reaching the surface, indicating the scattering and absorption of anthropogenic aerosols. Over the inland, the radiation flux is slightly increased (mostly not significant statistically). This is mainly due to the longwave emission of absorbing aerosols. In contrast, the pattern of indirect (cloud) radiative forcing (ΔCRF, Fig. 7d–f) varies significantly with time. Note that three kinds of processes contribute to ΔCRF. First, increased aerosols reduce the clear-sky shortwave fluxes, which generally weakens cloud effects; second, increased aerosols increase cloud albedo by acting as cloud nuclei and enhance cloud radiative forcing; third, cloud fraction might increase or decrease to adjust to changes in aerosol radiative effects and the associated circulation, which can either increase or decrease cloud radiative forcing. For example, the cooling over central China in Fig. 7e is mainly

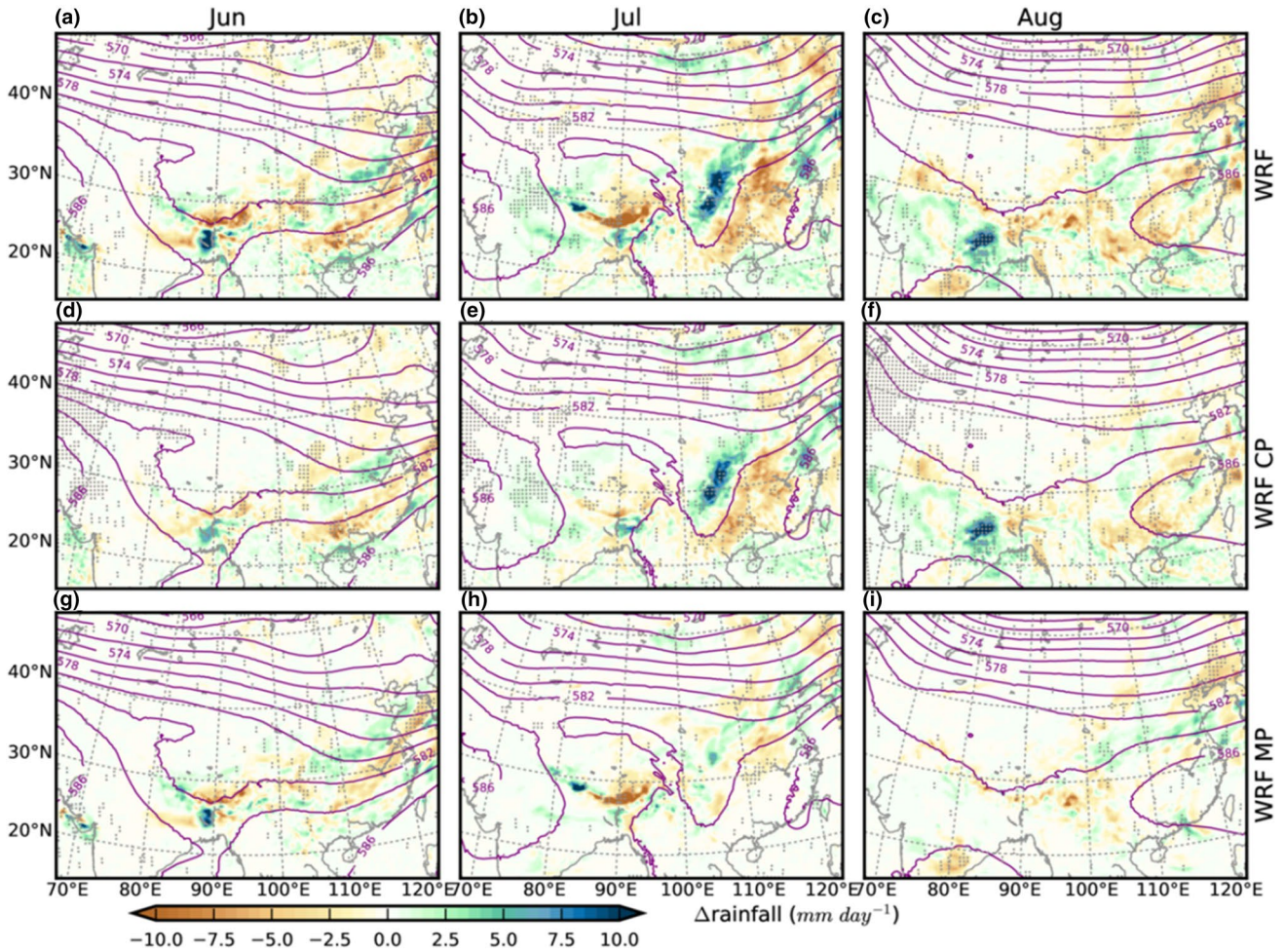

Fig. 5 Changes of rain rate at the surface due to the increased anthropogenic aerosols (control minus sensitivity): **a–c** total rain rate; **d–f** rain rate from cumulus parameterization; and **g–i** rain rate from microphysical parameterization. In this figure and Figs. 6, 7 and 8, *dots* indicate changes that are statistically significant (t test; P value < 0.1)

attributed to increased cloud fraction, while the warming to its east is attributed to decreased cloud fraction and decreased clear-sky radiation fluxes. The total radiative forcing associated with the aerosol perturbation is the general cooling over the eastern China with several warming (or less cooling) spots embedded over the WNPSH occupied regions.

Figure 8 presents circulation changes using the 850 hPa winds and the 500 hPa geopotential height fields. It shows increased geopotential heights over the eastern China, especially at the front of the WNPSH. This indicates that the WNPSH is westward extended. Consequently, the WNPSH occupied regions are featured with weakened southerlies (i.e. anomalous northerlies over the southeast China) and divergent flows, while to the west and north of the WNPSH are strengthened southerlies and convergent flows due to increased pressure gradients.

Given changes in precipitation, clouds, aerosol radiative forcing and circulation shown above, the following feedback processes are speculated to explain the intraseasonal characteristics of aerosol effects. First, the increased anthropogenic aerosols over the eastern China cool the surface via the solar dimming effect; the pressure increases over the eastern China, and the WNPSH is extended westward; less water vapor gets to the WNPSH occupied regions due to anomalous divergent flows (weakened monsoon) and produces less cloud and precipitation (low-level clouds might be increased due to increased atmospheric stability), while more water vapor gets to the west and north of the WNPSH due to anomalous convergent flows and produces more precipitation and clouds there, which cools the surface and further extends the WNPSH westward. Note that here the WNPSH is just slightly perturbed by the aerosol loading over the eastern China. Its intraseasonal migration is still

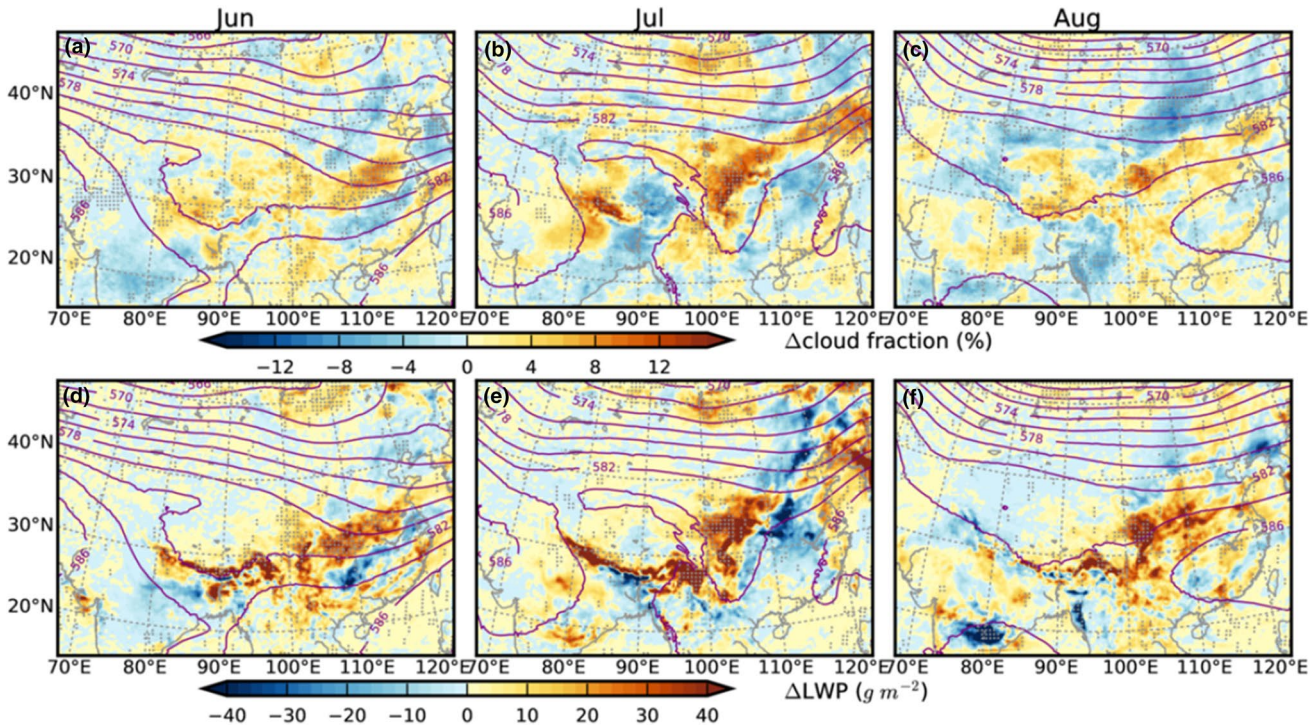

Fig. 6 Changes of cloud fraction (below 440 hPa) and liquid water path due to the increased anthropogenic aerosols (control minus sensitivity)

dominated by larger- and longer-scale climate processes (e.g., solar annual cycle, ENSO, PDO).

4.2 Interannual variability of the western North-Pacific subtropical high

The interannual variability of the EASM can be generally represented by that of the WNPSH (Chang et al. 2000; Wang et al. 2013a). Here we go further by using the westmost point in the 5880 contour (hereafter W588) of 500 hPa to indicate the WNPSH migration, for the 5880 contour is usually a closed circle and easy to be identified. Shown in Fig. 9, the W588 is usually located around 20°N in June, marches northwestward in July and retreats eastward in August. However, the marching path varies greatly between years. Note that the W588 can indicate the monsoon strength to some degree, but it is not a perfect indicator. For all years shown above, the monsoon rainfall over East Asia is generally tied with the 5860 contour, but the distance between 5880 and 5860 contours varies a lot in both longitudinal and latitudinal dimensions between years, so the W588 cannot precisely indicate how much the WNPSH gets deep into the continent. To save space, we select to show results of 6 months during 2002–2007, in which W588 locations show relatively large deviations from those in 2008. The six months are June of 2004 and 2006, July of 2002 and 2003, and August of 2005 and 2007.

Figure 10 presents responses of the monthly-mean rainfall at the surface and the 500 hPa geopotential height fields to increased anthropogenic aerosols. As the WNPSH occupies different regions for the selected months, which stands for different monsoon strengths, aerosol-induced changes of rainfall and circulation show large interannual variations (especially for subregions over the eastern China, e.g., North China), but the pattern of changes is always tied to the WNPSH location. The geopotential height in the front of the WNPSH is increased, indicating the westward extending of the WNPSH, which reduces precipitation over the WNPSH occupied region and enhances precipitation over regions to the west and north of the WNPSH. This is consistent with results from simulations of 2008, and confirms the intraseasonal characteristics of aerosol effects shown above.

While responses of the monthly-mean rainfall exhibit strong modulation by the intraseasonal migration of the WNPSH, responses of the summer-gross rainfall vary significantly (Fig. 11) due to interannual variability of the WNPSH migration path. However, a common feature is the generally wetter and dryer over the western and eastern China (especially the wetter over the northwest China and the dryer over the southeast China), respectively. From south to north, boundaries between the wetter and dryer regions are associated with how deep the WNPSH gets westward into the inland China. For example, the

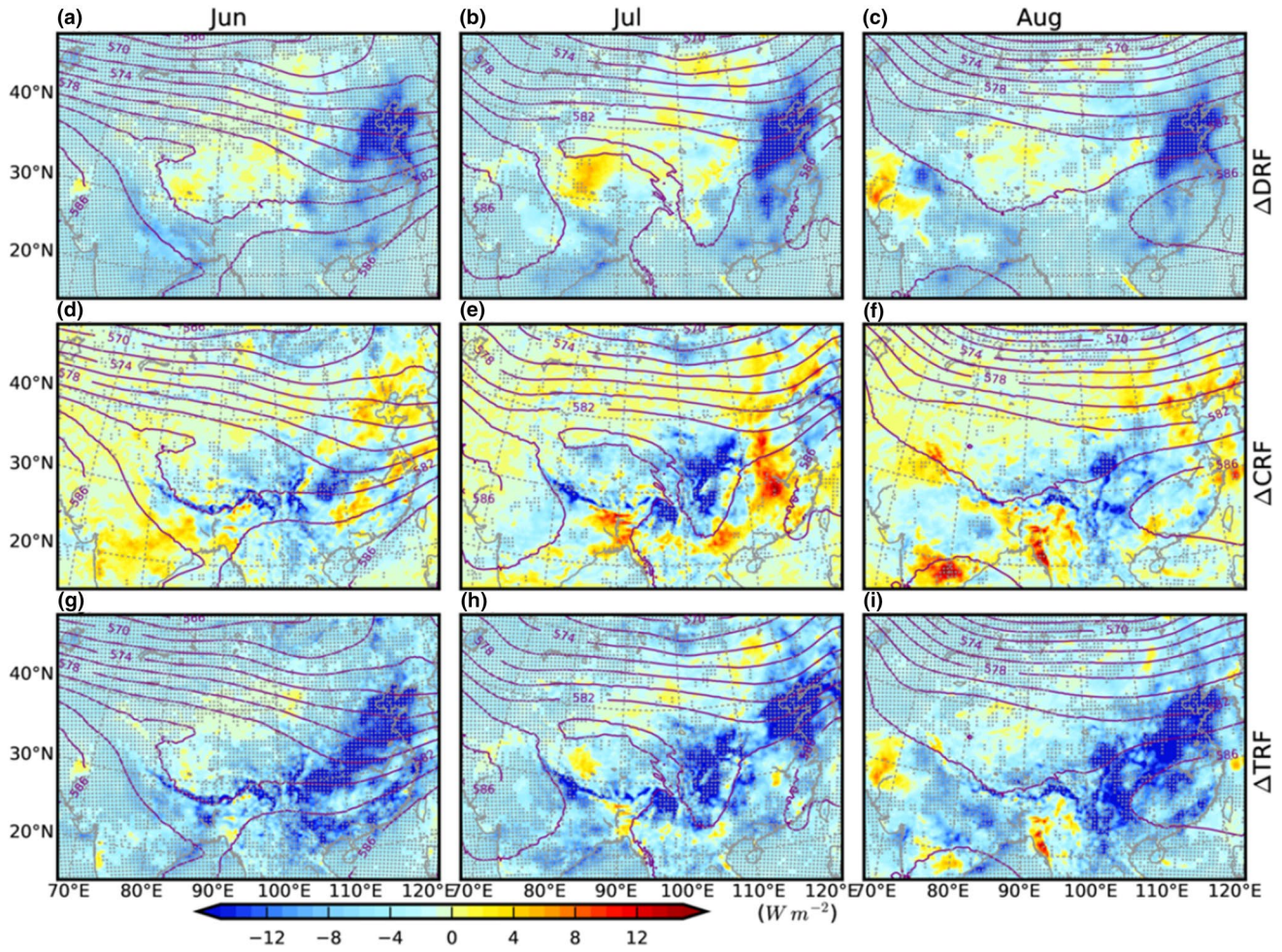

Fig. 7 Changes of radiative forcing at the surface due to increased anthropogenic aerosols (control minus sensitivity): **a–c** direct radiative forcing (DRF), **d–f** cloud radiative forcing (CRF) and **g–i** total radiative forcing (TRF). Both longwave and shortwave fluxes are included in the calculation, and the shortwave radiative effect dominates

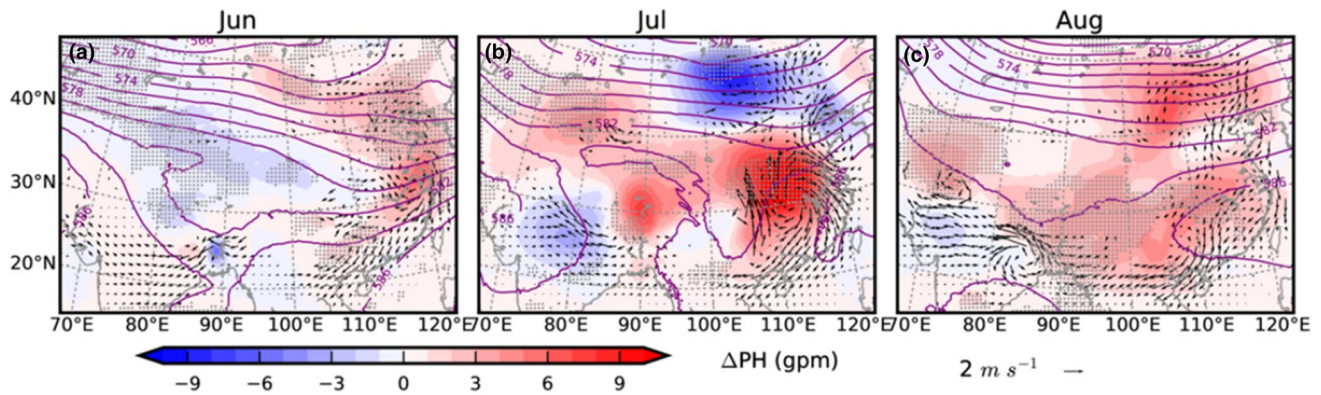

Fig. 8 Changes of the 500 hPa geopotential height fields (*shading* ΔPH) and the 850 hPa circulation (vectors) due to the increased anthropogenic aerosols (control minus sensitivity). Only wind vectors that are larger than 0.1 m s^{-1} are plotted

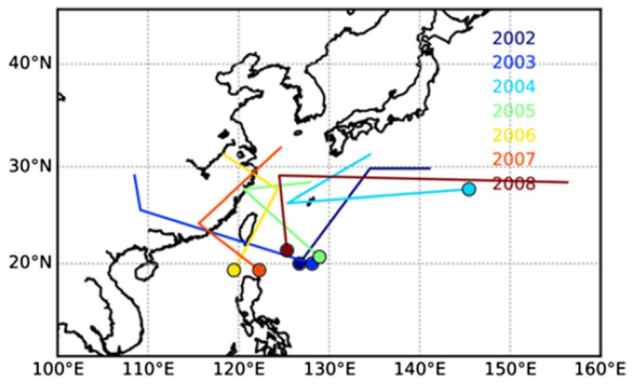

Fig. 9 Interannual variability of the western North-Pacific subtropical high (WNPSH) migration path in summers of 2002–2008, indicated by the location of the westmost point in the 5880 contour of 500 hPa (W588). The *filled dots* indicate W588 locations in June

boundaries in North China lie around 115°E in 2002 and 2004 when the W588 stays far from the continent in August; in contrast, the boundaries in South China are pushed westward to the TP region in 2003, 2006 and 2007 when the W588 gets on the continent occasionally.

5 Conclusion and discussion

This study investigates intraseasonal responses of the East Asia summer rainfall to the increased anthropogenic aerosols using multiple-year (2002–2008) WRF simulations, in which both direct and indirect effects of aerosols are calculated online with prescribed multi-component aerosol fields. Even though aerosol effects of precipitation suppression and convection invigoration are not fully accounted for due to the coarse horizontal resolution, the responses are still significant. Major findings are highlighted here. First, the spatial pattern of responses is tied to the WNPSH location (i.e. the rainfall is enhanced over regions to the west and north of the WNPSH and reduced over the WNPSH occupied region), and exhibits strong variations due to intraseasonal and interannual variability of the WNPSH migration. This implies that the WNPSH evolution has to be evaluated first when examining regional characteristics of aerosol effects over East Asia using general circulation models, in which the WNPSH is simulated rather than prescribed as in this study. Second, the WNPSH is shown to be westward extended by aerosol forcings over East Asia. Although it is accompanied by significant changes in rainfall and circulation, this extension is only a small perturbation at the intraseasonal scale to the WNPSH, whose migration is dominated by larger- and longer-scale processes. For example, the periodical oscillations in SST are responsible for most of the WNPSH variations (Chang et al. 2000; Ren

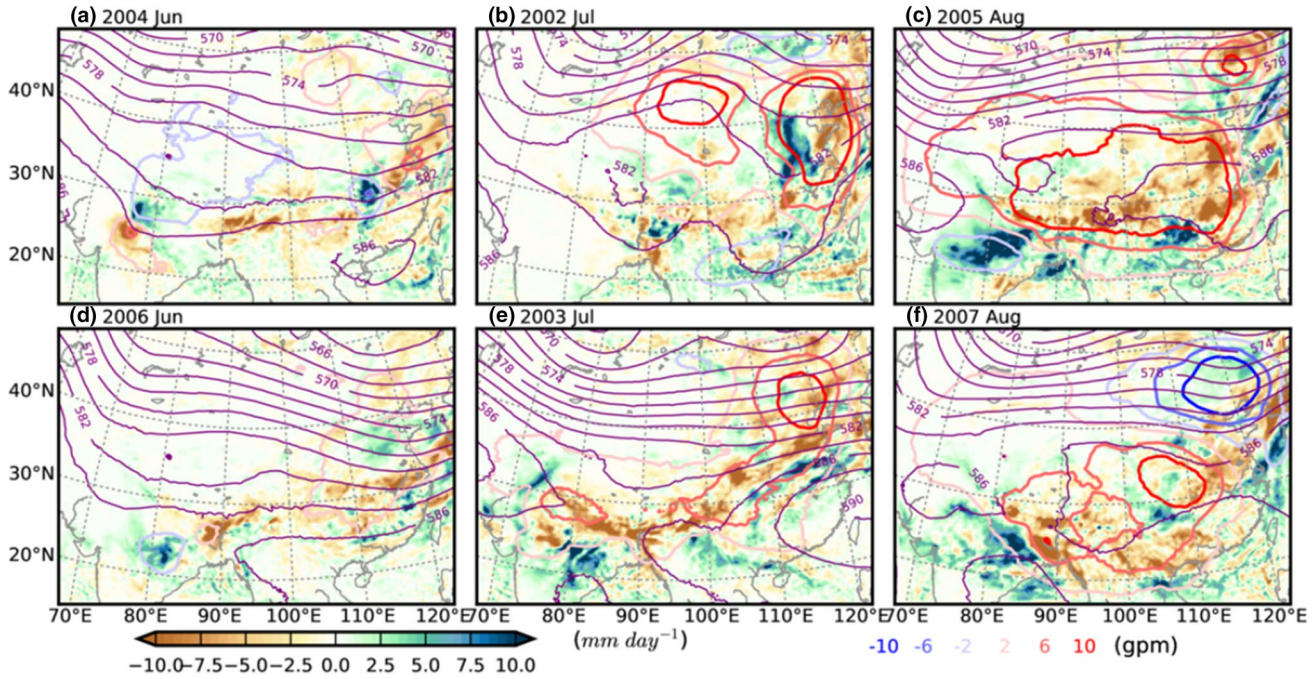

Fig. 10 Monthly-mean responses of the surface rain rate and the 500 hPa geopotential height field to increased anthropogenic aerosols for selected months during 2002–2007

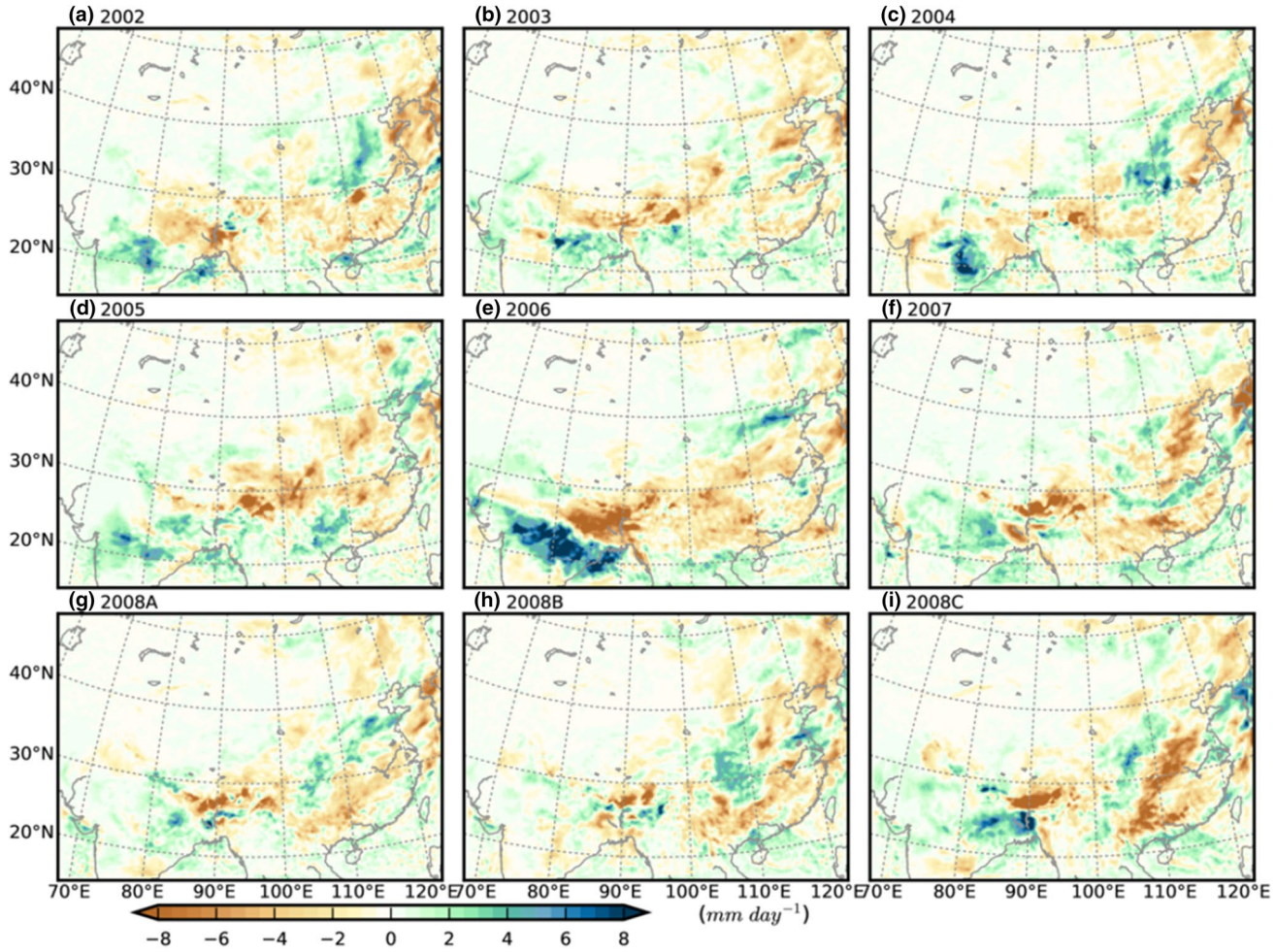

Fig. 11 Spatial patterns of the summer-mean response in rain rate at the surface: **a–f** results from simulations of 2002–2007; **g–i** results from the three pairs of simulations included in the ensemble of 2008. 2008A and 2008B were initialized from 2008-05-28 00:00:00 and 2008-05-26 12:00:00, respectively, while 2008C was initialized from 2008-05-28 00:00:00 but run on a second computer

et al. 2013), which is beyond the scope of this study. Third, responses of the summer-gross rainfall show a general pattern of more rainfall over the western China and less over the eastern China. This finding agrees with observational studies showing that it is getting wetter over the northwest China but dryer over the southeast China in the past few decades (Zhai et al. 2005; Feng and Zhao 2015).

As many precipitating systems over the eastern China originate from TPV vortices, the simulated TPV activities and their responses to the aerosol loading are also examined in this study. First, the TPVs do show modulations by the quasi-biweekly oscillation over the TP, but the phase correlation is not as clear (figure not shown) as shown by Zhang et al. (2014). This might be due to differences in the TPV detecting procedure. Second, TPVs are less frequently identified in the control case than in the sensitivity case for all pairs of simulations except 2008B (shown in Table 1). This tendency is consistent with the finding of Lin (2015) that TPV numbers shows a decreasing trend (though not very significant) since 1979. It is not sure whether this is induced by aerosol changes in China or India (or both), but it suggests a new possible path in which aerosols are modulating the summer rainfall over the eastern China. More effort is warranted to verify this and sort out the detailed mechanism.

Previous studies (Schneider and Bordoni 2008; Bordoni and Schneider 2008) showed that monsoons are mainly governed by feedbacks between large-scale extratropical eddies and tropical overturning circulation, wherein the former are generally carried by the midlatitude intraseasonal variations (e.g., Roundy 2012; Park et al. 2015). Within this context, the significant intraseasonal responses of EASM to aerosol perturbations revealed in this study indicate that the intraseasonal scale could be a breakthrough point for understanding aerosol-monsoon interactions.

Table 1 Total frequency of low-level cyclones on the Tibet Plateau in the summer of all simulations

	2002	2003	2004	2005	2006	2007	2008A	2008B	2008C
Control	969	837	1062	1033	771	925	1198	1171	1156
Sensitivity	1092	900	1124	1176	924	948	1242	1156	1228

The low-level cyclones are identified on the 3-hourly 500 hPa surface with two criterions. First, the low-pressure center is circled by one or more closed contours that are plotted every 5 gpm; second, the outermost closed contour covers an area no less than 10,000 km^2. This method was ever used in Lin (2015) to identify and track TPVs in the ERA-Interim reanalysis. Note that numbers in this table are not normalized with respect to sampling frequency (eight times per day) and simulation length (92 days), and that the lifetime criterion which requires tracking TPV propagation is not applied, so the numbers cannot be directly compared with TPV numbers in Lin (2015)

Acknowledgements The authors thank the two anonymous reviewers for valuable suggestions and comments, which greatly help clarify this study. This study is supported by a grant from the Office of Sciences (BER), U.S. DOE. JY acknowledges the supports by funds from National Natural Science Foundation of China (Grant 41375003 and Grant 41621061), and WCW acknowledges the supports of Chinese 973 program (Grant 2013CB955803) to visit Beijing University and the Institute of Atmospheric Physics.

References

Albrecht BA (1989) Aerosols, cloud microphysics, and fractional cloudiness. Science 245:1227–1230. doi:10.1126/science.245.4923.1227

Bordoni S, Schneider T (2008) Monsoons as eddy-mediated regime transitions of the tropical overturning circulation. Nat Geosci 1:515–519. doi:10.1038/ngeo248.

Chang C-P, Zhang Y, Li T (2000) Interannual and interdecadal variations of the East Asian summer monsoon and tropical Pacific SSTs. Part I: roles of the subtropical ridge. J Climate 13:4310–4325. doi:10.1175/1520-0442(2000)013<4310:IAIVOT>2.0.CO;2

Chen F, Dudhia J (2001) Coupling an advanced land surface–hydrology model with the Penn State–NCAR MM5 modeling system. Part I: model implementation and sensitivity. Mon Weather Rev 129:569–585. doi:10.1175/1520-0493(2001)129<0569:caalsh>2.0.co;2

Chen J-P, Liu S-T (2004) Physically based two-moment bulkwater parametrization for warm-cloud microphysics. Q J Roy Meteor Soc 130:51–78. doi:10.1256/Qj.03.41

Chen G, Wang W-C (2016) Aerosol–stratocumulus–radiation interactions over the southeast Pacific: implications to the underlying air–sea coupling. J Atmos Sci 73:2759–2771. doi:10.1175/JAS-D-15-0277.1

Chen G, Wang W-C, Chen J-P (2015) Aerosol–stratocumulus–radiation interactions over the southeast Pacific. J Atmos Sci 72:2612–2621. doi:10.1175/jas-d-14-0319.1

Cheng C-T, Wang W-C, Chen J-P (2007) A modelling study of aerosol impacts on cloud microphysics and radiative properties. Q J Roy Meteor Soc 133:283–297. doi:10.1002/Qj.25

Cheng C-T, Wang W-C, Chen J-P (2010) Simulation of the effects of increasing cloud condensation nuclei on mixed-phase clouds and precipitation of a front system. Atmos Res 96:461–476. doi:10.1016/j.atmosres.2010.02.005

Dao S-Y, Chen L-S (1957) The structure of general circulation over continent of Asia in summer. J Meteorol Soc Japan Ser II(35A):215–229

Dee DP et al (2011) The ERA-Interim reanalysis: configuration and performance of the data assimilation system. Q J Roy Meteor Soc 137:553–597. doi:10.1002/qj.828

Fan J et al (2012) Aerosol impacts on clouds and precipitation in eastern China: Results from bin and bulk microphysics. J Geophys Res Atmos 117:D00K36. doi:10.1029/2011jd016537

Fan J, Wang Y, Rosenfeld D, Liu X (2016) Review of aerosol–cloud interactions: mechanisms, significance, and challenges. J Atmos Sci 73:4221–4252. doi:10.1175/jas-d-16-0037.1

Feng Y, Zhao X (2015) Changes in spatiotemporal pattern of precipitation over China during 1980–2012. Environ Earth Sci 73:1649–1662. doi:10.1007/s12665-014-3517-x.

Guo L, Highwood EJ, Shaffrey LC, Turner AG (2013) The effect of regional changes in anthropogenic aerosols on rainfall of the East Asian Summer Monsoon. Atmos Chem Phys 13:1521–1534. doi:10.5194/acp-13-1521-2013

Hong S-Y, Noh Y, Dudhia J (2006) A new vertical diffusion package with an explicit treatment of entrainment processes. Mon Weather Rev 134:2318–2341. doi:10.1175/mwr3199.1

Hong C-C, Lee M-Y, Hsu H-H, Kuo J-L (2010) Role of submonthly disturbance and 40–50 day ISO on the extreme rainfall event associated with Typhoon Morakot (2009) in Southern Taiwan. Geophys Res Lett 37:L08805. doi:10.1029/2010gl042761

Huffman GJ et al (2001) Global precipitation at one-degree daily resolution from multisatellite observations. J Hydrometeorol 2:36–50. doi:10.1175/1525-7541(2001)002<0036:gpaodd>2.0.co;2

Iacono MJ, Delamere JS, Mlawer EJ, Shephard MW, Clough SA, Collins WD (2008) Radiative forcing by long-lived greenhouse gases: Calculations with the AER radiative transfer models. J Geophys Res Atmos. doi:10.1029/2008JD009944.

Kain JS (2004) The Kain–Fritsch convective parameterization: an update. J Appl Meteorol 43:170–181. doi:10.1175/1520-0450(2004)043<0170:tkcpau>2.0.co;2

Lamarque JF et al (2012) CAM-chem: description and evaluation of interactive atmospheric chemistry in the Community Earth System Model. Geosci Model Dev 5:369–411. doi:10.5194/gmd-5-369-2012

Lau KM, Kim KM (2006) Observational relationships between aerosol and Asian monsoon rainfall, and circulation. Geophys Res Lett 33:L21810. doi:10.1029/2006gl027546

Lau KM, Kim MK, Kim KM (2006) Asian summer monsoon anomalies induced by aerosol direct forcing: the role of the Tibetan Plateau. Clim Dynam 26:855–864. doi:10.1007/s00382-006-0114-z

Li Z, Niu F, Fan J, Liu Y, Rosenfeld D, Ding Y (2011a) Long-term impacts of aerosols on the vertical development of clouds and precipitation. Nat Geosci 4:888–894. doi:10.1038/Ngeo1313.

Li Z et al (2011b) East Asian studies of tropospheric aerosols and their impact on regional climate (EAST-AIRC): an overview. Journal of Geophysical Research: Atmospheres 116:D00K34. doi:10.1029/2010jd015257

Li S et al (2016a) Impact of aerosols on regional climate in southern and northern China during strong/weak East Asian summer monsoon years. J Geophys Res Atmos. doi:10.1002/2015jd023892

Li Z et al (2016b) Aerosol and monsoon climate interactions over Asia. Rev Geophys. doi:10.1002/2015rg000500.

Lin Z (2015) Analysis of Tibetan Plateau vortex activities using ERA-Interim data for the period 1979–2013. J Meteorol Res 29:720–734. doi:10.1007/s13351-015-4273-x

Liu H, Yang J, Zhang D-L, Wang B (2014) Roles of synoptic to quasi-biweekly disturbances in generating the summer 2003 heavy rainfall in East China. Mon Weather Rev 142:886–904. doi:10.1175/MWR-D-13-00055.1

Manoj MG, Devara PCS, Safai PD, Goswami BN (2011) Absorbing aerosols facilitate transition of Indian monsoon breaks to active spells. Clim Dynam 37:2181–2198. doi:10.1007/s00382-010-0971-3

Monin AS, Obukhov AM (1954) Basic laws of turbulent mixing in the surface layer of the atmosphere. Contrib Geophys Inst Slovak Acad Sci 24:163–187

Park H-S, Lintner BR, Boos WR, Seo K-H (2015) The effect of mid-latitude transient eddies on monsoonal southerlies over Eastern China. J Climate 28:8450–8465. doi:10.1175/jcli-d-15-0133.1

Qian W, Lee DK (2000) Seasonal march of Asian summer monsoon. Int J Climatol 20:1371–1386. doi:10.1002/1097-0088(200009)20:11<1371::AID-JOC538>3.0.CO;2-V

Ramanathan V, Crutzen PJ, Kiehl JT, Rosenfeld D (2001) Atmosphere—Aerosols, climate, and the hydrological cycle. Science 294:2119–2124. doi:10.1126/science.1064034

Ren X, Yang X, Sun X (2013) Zonal oscillation of western Pacific subtropical high and subseasonal SST variations during Yangtze persistent heavy rainfall events. J Climate 26:8929–8946. doi:10.1175/JCLI-D-12-00861.1

Rosenfeld D et al (2008) Flood or drought: How do aerosols affect precipitation? Science 321:1309–1313. doi:10.1126/science.1160606

Roundy PE (2012) Tropical–extratropical interactions. In: Lau WKM, Waliser DE (eds) Intraseasonal variability in the atmosphere-ocean climate system. second edn. Springer, Berlin, pp 497–512. doi:10.1007/978-3-642-13914-7_14

Schneider T, Bordoni S (2008) Eddy-mediated regime transitions in the seasonal cycle of a Hadley circulation and implications for monsoon dynamics. J Atmos Sci 65:915–934. doi:10.1175/2007jas2415.1

Stevens B, Feingold G (2009) Untangling aerosol effects on clouds and precipitation in a buffered system. Nature 461:607–613. doi:10.1038/nature08281

Tao S-y, Ding Y-h (1981) Observational evidence of the influence of the Qinghai-Xizang (Tibet) Plateau on the Occurrence of heavy rain and severe convective storms in China. Bull Amer Meteorol Soc 62:23–30. doi:10.1175/1520-0477(1981)062<0023:oeotio>2.0.co;2

Thiébaux J, Rogers E, Wang W, Katz B (2003) A new high-resolution blended real-time global sea surface temperature analysis. Bull Amer Meteorol Soc 84:645–656. doi:10.1175/BAMS-84-5-645

Thompson G, Tewari M, Ikeda K, Tessendorf S, Weeks C, Otkin J, Kong F (2016) Explicitly-coupled cloud physics and radiation parameterizations and subsequent evaluation in WRF high-resolution convective forecasts. Atmos Res 168:92–104. doi:10.1016/j.atmosres.2015.09.005

Twomey S (1974) Pollution and planetary albedo. Atmos Environ 8:1251–1256. doi:10.1016/0004-6981(74)90004-3

Wang M, Duan A (2015) Quasi-biweekly oscillation over the Tibetan Plateau and its link with the Asian summer monsoon. J Climate 28:4921–4940. doi:10.1175/jcli-d-14-00658.1

Wang B, Xiang B, Lee J-Y (2013a) Subtropical High predictability establishes a promising way for monsoon and tropical storm predictions. Proc Natl Acad Sci 110:2718–2722. doi:10.1073/pnas.1214626110

Wang Y, Khalizov A, Levy M, Zhang RY (2013b) New directions: Light absorbing aerosols and their atmospheric impacts. Atmos Environ 81:713–715. doi:10.1016/j.atmosenv.2013.09.034

Wang Y et al (2014) Assessing the effects of anthropogenic aerosols on Pacific storm track using a multiscale global climate model. Proc Natl Acad Sci 111:6894–6899. doi:10.1073/pnas.1403364111

Wang Y, Jiang J, Su H (2015) Atmospheric responses to the redistribution of anthropogenic aerosols. J Geophys Res Atmos. doi:10.1002/2015jd023665

Yang J, Wang B, Bao Q (2010) Biweekly and 21-30-day variations of the subtropical summer monsoon rainfall over the lower reach of the Yangtze River Basin. J Climate 23:1146–1159. doi:10.1175/2009JCLI3005.1

Yang X, Ferrat M, Li Z (2013a) New evidence of orographic precipitation suppression by aerosols in central China. Meteorol Atmos Phys 119:17–29. doi:10.1007/s00703-012-0221-9

Yang X, Yao Z, Li Z, Fan T (2013b) Heavy air pollution suppresses summer thunderstorms in central China. J Atmos Sol-Terr Phy 95–96:28–40. doi:10.1016/j.jastp.2012.12.023

Yang J, Bao Q, Wang B, Gong D, He H, Gao M (2014) Distinct quasi-biweekly features of the subtropical East Asian monsoon during early and late summers. Clim Dynam 42:1469–1486. doi:10.1007/s00382-013-1728-6

Yang J, Bao Q, Wang B, He H, Gao M, Gong D (2016) Characterizing two types of transient intraseasonal oscillations in the Eastern Tibetan Plateau summer rainfall. Clim Dynam. doi:10.1007/s00382-016-3170-z

Zhai P, Zhang X, Wan H, Pan X (2005) Trends in total precipitation and frequency of daily precipitation extremes over China. J Climate 18:1096–1108. doi:10.1175/JCLI-3318.1

Zhang P, Li G, Fu X, Liu Y, Li L (2014) Clustering of Tibetan Plateau vortices by 10–30-Day intraseasonal oscillation. Mon Weather Rev 142:290–300. doi:10.1175/mwr-d-13-00137.1